Proceedings of the 17th World Congress
The International Federation of Automatic Control
Seoul, Korea, July 6-11, 2008

Adaptive Vision-Based Controller for Small Rotorcraft UAVs Control and Guidance

Farid Kendoul, **Isabelle Fantoni** and **Rogelio Lozano**

Laboratoire Heudiasyc, CNRS-UTC, 60200 Compiègne, France
(Tel: 00333 44 23 49 54; e-mail: fkendoul@hds.utc.fr),
(e-mail: ifantoni@hds.utc.fr) and (e-mail: rlozano@hds.utc.fr)

Abstract: The design of a reliable control and guidance system for aerial vehicles based only on visual information and Inertial Measurement Unit (IMU) data possesses many unsolved challenging problems, ranging from hardware and software development to pure control-theoretical issues. Theses issues have been addressed by proposing a bio-inspired adaptive autopilot for self-localization, obstacles detection and control of small autonomous rotorcraft using optic flow and IMU measurements. This paper focuses particulary on the design of a hierarchical adaptive control system. Adaptive control tools have been used to recover the absolute aircraft velocities and real distances to obstacles. These estimates are then exploited by a multipurpose hierarchical controller for achieving various navigational tasks such as take-off, hovering, trajectory tracking and vertical landing. Furthermore, the asymptotic stability of the entire closed-loop system has been established using connected systems control theories. Simulation results over various ranges of the flight envelope illustrate that the proposed autopilot performs very well and allows a simulated rotorcraft UAV to achieve interesting flight behaviours.

Keywords: Adaptive control, rotorcraft UAVs, hierarchical flight control, vision-based control, bio-inspired navigation.

1. INTRODUCTION

Recently, there is a growing interest in developing fully autonomous Unmanned Aerial Vehicles (UAVs) for military and civilian applications. The design of sensing, control and navigation systems is a crucial step in the development of such flying machines. Altitude, position and orientation measurements are usually sufficient for UAVs operating at high altitudes. Therefore, conventional Inertial Navigation Systems (INS) that include pressure sensor, GPS and IMU provide the needed information for flight control and waypoint navigation. On the other hand, small and micro UAVs are designed to operate at low altitude in cluttered environments. To achieve this kind of missions, the UAV needs to detect and avoid obstacles in real-time, recognize and track targets, map the environment and plan its path. Environment perception technologies used within UAVs include cameras and range sensors. For some particular operations such as autonomous landing, range sensors (laser, pressure and ultrasonics) are widely used. However, computer vision plays the most important role in several applications. Indeed, computer vision provides a viable and useful solution to sensing on UAVs because cameras are too light to fit the limited payload capabilities of small UAVs. Although computer vision has many benefits for UAVs control and guidance, it presents many challenges too. Indeed, the design of reliable and real-time vision algorithms is a complex problem. Moreover, synthesizing robust flight controllers that are based on visual cues is a challenging task.

Despite these challenging issues, promising results have been obtained using computer vision for aerial vehicles control and navigation. Potential applications of computer vision for UAVs include aircraft self-motion recovery, obstacles detection, depth map reconstruction, target detection and tracking. The existing vision strategies for achieving these tasks can be classified in different manners. Here, we make a distinction between vision approaches that rely on image content (visual features) and vision strategies that are based on image motion (optic flow) regardless its content. Image content-based methods aim at detecting known features in the image such as artificial marks, Shakernia et al. (2002), horizon Ettinger et al. (2003) or known objects like windows Saripalli et al. (2005), roads, etc. On the other hand, many researchers have been interested in using image motion for UAVs control and guidance, Amidi et al. (1999). One of the main advantage of these approaches is their suitability for unknown and unstructured environments. Furthermore, recent findings on insects flight revealed that these latter rely heavily on optic flow for flight control and navigation Srinivasan et al. (1996). These findings have motivated many researchers to design insect-inspired optic flow-based autopilots for small flying machines Ruffier and Franceschini (2005); Zufferey and Floreano (2006); Green et al. (2004).

In this paper, we present a practical autopilot which takes inspiration from flying insects. It is based on a monocular camera and an IMU and it includes a vision module for localization and 3D terrain modeling, and an adaptive control system for navigation and trajectory tracking. Functionally, the vision algorithm computes in real time the optic flow, fuses the visual and angular rate data, and recovers the aircraft ego-motion and depth map

modulo some unknown scale factor (see Kendoul et al. (2007) for more details in the vision system). Therefore, we formulate the vision-based control problem as the control of a nonlinear system with unknown parameters (scale factor). An adaptive observer has been used to recover the absolute aircraft velocities and real distances to obstacles. These estimates are then, exploited by a multipurpose hierarchical controller for autonomous take-off, hovering, trajectory tracking and vertical landing.

Although previous works have shown that visual cues can lead to an autonomous flight, our work has extended this finding in a number of areas. Firstly, the proposed autopilot is based on only two lightweight sensors, a small monocular camera and a low-cost IMU. Secondly, system identification techniques have been applied to estimate the unknown scale factor introduced by visual measurements, thereby recovering the absolute UAV motion and real depth map. Furthermore, we have considered the 3D flight control problem without any restrictions on the UAV motion. Finally, the asymptotic stability of the entire connected system has been established using advanced nonlinear control theories.

The remainder of this paper is organized as follows: section 2 outlines and formulates the problem of UAVs control using visual cues and IMU data. In section 3, we present the proposed adaptive flight controller followed by the stability analysis for the closed-loop system. Numerical results using synthetic environments and a simulated UAV are presented in Section 4. Finally, some conclusions are given in Section 5.

2. MATHEMATICAL FORMULATION OF THE OPTIC FLOW-BASED CONTROL PROBLEM

It is common to represent the control problem by differential equations that model the plant (UAV) dynamics, and an algebraic system that expresses the available measurements as functions of state variables. Let us denote by $(\xi, \upsilon, \eta, \dot{\eta})$ the position, translational velocity, orientation and angular rate vectors, respectively. Therefore, the dynamics of a rotorcraft UAV such as the quadrotor helicopter can be represented by the following mathematical model, Kendoul (2007):

$$\begin{cases} \ddot{\xi} = \dfrac{1}{m} u R e_3 - g e_3 \\ M(\eta)\ddot{\eta} + C(\eta, \dot{\eta})\dot{\eta} = \Psi(\eta)^T \tau \end{cases} \quad (1)$$

where u is the total thrust, τ is the torque vector, R and Ψ are the rotation and Euler matrices, respectively. The pseudo-inertial matrix $M(\eta)$ and the centripetal vector $C(\eta, \dot{\eta})$ are defined in Kendoul (2007).

Since the rotational dynamics are feedback linearizable, we propose the following change of variables:

$$\tau = J\Psi(\eta)\tilde{\tau} + \Psi^{-1} C(\eta, \dot{\eta})\dot{\eta} \quad (2)$$

which is invertible for $\theta \neq k\pi/2$.

By recalling (1) and (2), the optic flow-based control problem can be formulated as follows:

$$\begin{cases} \dot{\xi} = \upsilon \\ \dot{\upsilon} = \dfrac{1}{m} u R e_3 - g e_3 \\ \ddot{\eta} = \tilde{\tau} \end{cases}, \quad \begin{cases} y_z = b\, z \in \mathcal{R} \\ Y_\upsilon = b\, \upsilon \in \mathcal{R}^3 \\ Y_\eta = (\eta, \dot{\eta})^T \in \mathcal{R}^6 \end{cases} \quad (3)$$

The available measurements, provided by the vision-IMU system, are denoted by $(y_z, Y_\upsilon, Y_\eta)$. In fact, we have developed a bio-inspired sensing system that is based on a monocular camera and a small IMU. Then, a real-time vision algorithm has been designed for image motion computation and interpretation. Fusing optic flow and angular rate data allowed to estimate the UAV velocities and distances to obstacles modulo some unknown scale factor $b \in \mathbb{R}^+ - \{0\}$. If we assume that the camera is down-looking, then the extracted distances are proportional to the aircraft altitude z (height map).

From (3), one can observe that there is no direct information about the horizontal position (x, y). Moreover, the translational velocity vector υ and the UAV altitude z are not known explicitly. They are measured modulo some unknown scale factor b. Hence, the *position-based control* scheme can not be directly used because the aircraft position and velocity can not be estimated using only the available measurements. The *image-based control* approach is also not suitable because it complicates the control design and may limit the flight envelope to special cases. Our objective is to design a practical multipurpose controller that can achieve many navigational tasks using IMU data and the information extracted from optic flow. We have thus, proposed a framework that can be considered as the combination of the *position- and image-based control* schemes. In fact, we use the visual cues to partially extract information about the aircraft position and orientation $(y_z, Y_\upsilon, Y_\eta)$, and the state variables are reconstructed by the controller itself. In other words, the measurements are expressed in terms of visual signals and the control task is defined in terms of aircraft position and orientation.

Let $z_d(t) \in \mathbb{R}^1$, $\upsilon_d(t) \in \mathbb{R}^3$ and $\psi_d(t) \in \mathbb{R}^1$ be the desired trajectories. The control strategy aims then, at finding a feedback control $u(y_z, Y_\upsilon, Y_\eta, z_d, \upsilon_d)$ and $\tilde{\tau}(y_z, Y_\upsilon, Y_\eta, z_d, \upsilon_d, \psi_d)$ such that the tracking errors $(z(t) - z_d(t), \upsilon(t) - \upsilon_d(t), \psi(t) - \psi_d(t)) \in \mathbb{R}^5$ are asymptotically stable for all initial conditions. In fact, information about the aircraft velocities and altitude is sufficient for achieving several navigational tasks. In addition, most of navigational tasks are expressed in terms of desired velocities, altitude and heading (yaw angle). Indeed, studies on insect's flight behaviours have revealed that these latter control their velocities for dealing with the navigation problem.

Insects like flies and bees use similar measurements (angular rate data and information extracted from optic flow such as self-motion and distances to obstacles) to deal with the 3D navigation problem. Thus, it is clear from the theoretical and practical points of view that many navigational tasks such as landing, translational flight regulation and terrain following can be achieved using the measurements given in (3). Furthermore, if the unknown parameter b can be estimated on-line, then more complex behaviours can be achieved. Indeed, we can stabilize the UAV at some desired altitude and make the rotorcraft follow some arbitrary trajectory. It is evident that the estimation of the unknown parameter b allows the recovery of the absolute velocity vector υ and the aircraft altitude z. Consequently, the optic flow-based control, usually used for reactive behaviours, can be extended to more complex navigational tasks. This constitutes the major motivation for augmenting a flight

controller by an identification algorithm and an adaptive mechanism.

In the next section, we will design an adaptive hierarchical controller that jointly identifies the unknown parameter b, recovers the state variables (z, υ) and stabilizes the tracking errors $z(t) - z_d(t)$, $\upsilon(t) - \upsilon_d(t)$ and $\psi(t) - \psi_d(t)$).

3. ADAPTIVE HIERARCHICAL 3D FLIGHT CONTROLLER

Since we are using a down-looking camera and an IMU, then, only aircraft attitude $(\eta, \dot{\eta})$, translational velocity υ and its altitude z can be accurately controlled. The considered model for the control design is thus, the following:

$$\begin{cases} \dot{z} = \upsilon_z \\ \dot{\upsilon} = \dfrac{1}{m} u R e_3 - g e_3 \\ \ddot{\eta} = \tilde{\tau} \end{cases}, \begin{cases} y_z = b\, z \\ Y_\upsilon = b\, \upsilon \\ Y_\eta = (\eta, \dot{\eta})^T \end{cases} \tag{4}$$

Consequently, the vision-based control of a rotorcraft UAV is formulated as the control of a nonlinear system with an unknown parameter. Therefore, various adaptive control tools can be applied. We have chosen to use the *indirect adaptive control* design because it has the advantage to be flexible since different identification algorithms can be combined with different control strategies. Furthermore, this control scheme has the advantage to separate the estimation and control processes, thereby facilitating the analysis of the closed-loop system stability.

The control design for system (4) is be addressed in three steps:

(1) Design an adaptive observer that identifies b and estimates the state variables (z, υ) using the input-output data.
(2) Synthesize a hierarchical flight controller that exploits the estimates $(\hat{z}, \hat{\upsilon})$ and the measurements $(\eta, \dot{\eta})$ to achieve the assigned control tasks.
(3) Analyze the closed-loop system stability and robustness.

3.1 Parameter identifier and adaptive observer

As a first step towards the design of an adaptive controller, we develop an adaptive observer that estimates the unknown parameter b and recovers that aircraft velocity vector υ and altitude z.

By recalling (3) and differentiating the measurement vector $Y_\upsilon = (y_{\upsilon_x}, y_{\upsilon_y}, y_{\upsilon_z})^T$ with respect to time, we obtain:

$$\begin{cases} \dot{y}_{\upsilon_x} = b\dot{\upsilon}_x = -b\,\dfrac{u}{m}\sin\theta \triangleq b\,\gamma_x \\ \dot{y}_{\upsilon_y} = b\dot{\upsilon}_y = b\,\dfrac{u}{m}\cos\theta\sin\phi \triangleq b\,\gamma_y \\ \dot{y}_{\upsilon_z} = b\dot{\upsilon}_z = b\,(\dfrac{u}{m}\cos\theta\cos\phi - g) \triangleq b\,\gamma_z \end{cases} \tag{5}$$

Since the Euler angles (ϕ, θ) are measured by the IMU, then, the signals $(\gamma_x, \gamma_y, \gamma_z)$ are available for the parameter identification algorithm. Furthermore, the variables $(\gamma_x, \gamma_y, \gamma_z)$ correspond to the aircraft translational accelerations which are directly available from the accelerometers contained in the IMU. The unknown parameter b can, thus, be accurately estimated from the input-output data (5) using a robust *Recursive Least Squares* (RLS) algorithm, Ioannou and Sun (1996); Kendoul (2007). In a deterministic case, b can be estimated using one of the following SISO subsystems "$\dot{y}_{\upsilon_i} = \gamma_i,\ i = x, y, z$". An interesting solution could consist in estimating b for each SISO subsystem and then, fuse the three obtained estimates $(\hat{b}_x, \hat{b}_y, \hat{b}_z)$ in a favorable manner. For more robustness against noise and external disturbances, we have applied the RLS algorithm with projection and dead-zone in order to estimate $\hat{b}_x, \hat{b}_y$ and $\hat{b}_z$ from $(y_{\upsilon_x}, \gamma_x)$, $(y_{\upsilon_y}, \gamma_y)$ and $(y_{\upsilon_z}, \gamma_z)$, respectively. The three estimates $(\hat{b}_x, \hat{b}_y, \hat{b}_z)$ have then been fused using a weighted averaging method where the weights depend on the *Persistency Excitation* (PE) property of each signal $\gamma_i,\ i = x, y, z$.

Theorem 1. For $i = x, y, z$, the modified RLS algorithm with projection and dead-zone guarantees the following properties, Ioannou and Sun (1996):

(a) $\hat{b}_i,\ \dot{\hat{b}}_i \in \mathcal{L}_\infty$ (bounded).
(b) $b_{min} \leq \hat{b}_i(t) \leq b_{max},\ \forall t \geq 0$, where $b_{min} > 0$ and $b_{max} > 0$ are a priori known lower and upper bounds of the parameter b (projection principle).
(c) $\lim_{t\to\infty} \hat{b}_i(t) = \bar{b}_i$ where $\bar{b}_i$ is a positive constant.
(d) If $\gamma_i \in \mathcal{L}_\infty$ and γ_i is ***PE***, then the estimate $\hat{b}$ converges exponentially to its true value [1] b.

Since the three estimates $(\hat{b}_x, \hat{b}_y, \hat{b}_z)$ satisfy the properties in Theorem 1, it is then trivial to show that $\hat{b}(t) > 0$ and satisfies also the same properties. Once the scale factor b is identified, the aircraft velocity vector υ and altitude z can be estimated as follows:

$$\hat{z} = \frac{1}{\bar{b}} y_z = \frac{b}{\bar{b}} z \quad \text{and } \hat{\upsilon} = \frac{1}{\bar{b}} Y_\upsilon = \frac{b}{\bar{b}} \upsilon_z \tag{6}$$

Proposition 2. The adaptive observer (6) is stable and the convergence of the state variables $(\hat{z}, \hat{\upsilon})$ is guaranteed. Furthermore, if the *PE* property is satisfied, then the estimation errors $(\tilde{z} = z - \hat{z}, \tilde{\upsilon} = \upsilon - \hat{\upsilon})$ converge to zero.

In fact, the observer stability is a direct consequence of the parameter identifier (RLS algorithm) stability. Indeed, the obtained estimates $(\hat{z}, \hat{\upsilon})$ satisfy the following properties:

- Since $\hat{b}(t) \in [b_{min}, b_{max}] \to \bar{b}$, then, from (6) we deduce that $(\hat{z}, \hat{\upsilon}) \to b/\bar{b}(z, \upsilon)$.
- Furthermore, if $(\gamma_x, \gamma_y, \gamma_z)$ satisfy the *PE* property, then, $\hat{b} \to \bar{b} = b$ which implies that $(\hat{z}, \hat{\upsilon}) \to (z, \upsilon)$.

3.2 Hierarchical flight controller design

Control design for rotorcraft UAVs is already a challenging task, especially when it comes to deal with unknown parameters and state variables estimation errors. To cope with these issues, we have proposed a hierarchical flight controller that is based on the inner-outer loop control scheme.

Let $\nu = q(u, \phi_d, \theta_d)^T = \frac{u}{m} R(\phi_d, \theta_d) e_3 - g e_3$ be a pseudo-control vector such that $(u, \phi_d, \theta_d)^T = q^{-1}(\nu)$ exists. By defining $\chi = (z - z_d, \upsilon - \upsilon_d)^T \in \mathcal{R}^4$ and $e = (\eta - \eta_d, \dot{\eta} - \dot{\eta}_d)^T \in \mathcal{R}^6$ as tracking errors, system (4) can be written in the following form:

[1] In the presence of external disturbances, $\tilde{b}_i = b - \hat{b}_i$ converges exponentially to the residual set: $\{\tilde{b}_i / |\tilde{b}_i| \leq c(\rho_0 + \bar{d})\}$, where $\bar{d}$ is the disturbance upper bound, c is a positive constant and ρ_0 characterizes the dead-zone.

$$\begin{cases} \dot{\chi} = A_1\chi + B_1(\nu - \dot{\upsilon}_d) + \underbrace{\dfrac{u}{m}H(\eta_d, e)}_{\Delta(u,\eta_d,e)} \\ \dot{e} = A_2 e + B_2(\tilde{\tau} - \ddot{\eta}_d) \end{cases} \quad (7)$$

where $H(\eta_d, e) = (0, h_x, h_y, h_z)^T$ is a nonlinear interconnection term (see Kendoul (2007) for the explicit expressions of its components). The matrices (A_1, B_1, A_2, B_2) are given by

$$A_1 = \begin{bmatrix} 0&0&0&1 \\ 0&0&0&0 \\ 0&0&0&0 \\ 0&0&0&0 \end{bmatrix}, A_2 = \begin{bmatrix} 0&0&0&1&0&0 \\ 0&0&0&0&1&0 \\ 0&0&0&0&0&1 \\ 0&0&0&0&0&0 \\ 0&0&0&0&0&0 \\ 0&0&0&0&0&0 \end{bmatrix}, B_1 = \begin{bmatrix} 0&0&0 \\ 1&0&0 \\ 0&1&0 \\ 0&0&1 \end{bmatrix}, B_2 = \begin{bmatrix} 0&0&0 \\ 0&0&0 \\ 0&0&0 \\ 1&0&0 \\ 0&1&0 \\ 0&0&1 \end{bmatrix}$$

The system (7) can be seen as two linear subsystems in cascade which are coupled by the nonlinear term $\Delta(u, \eta_d, e)$. As explained in Kendoul (2007), the inner-outer control scheme aims at synthesizing two control laws $\nu(\hat{\chi}, \dot{\upsilon}_d)$ and $\tilde{\tau}(e, \ddot{\eta})$ for controlling the aircraft position represented by the ξ-subsystem (outer-loop) and its orientation (inner-loop), i.e., the e-subsystem. Therefore, we choose

$$\begin{cases} \nu = -K_\chi\hat{\chi} + \dot{\upsilon}_d = -k_z(\hat{z} - z_d) - K_\upsilon(\hat{\upsilon} - \upsilon_d) + \dot{\upsilon}_d \\ \tilde{\tau} = -K_e e + \ddot{\eta}_d = -K_\eta(\eta - \eta_d) - K_{\dot{\eta}}(\dot{\eta} - \dot{\eta}_d) + \ddot{\eta}_d \end{cases} \quad (8)$$

where $K_\chi \in \mathcal{R}^{3\times4}$ and $K_e \in \mathcal{R}^{3\times6}$ are positive matrices such that $A_\chi = A_1 - B_1K_\chi$ and $A_e = A_2 - B_2K_e$ are Hurwitz.

In fact, the structural properties of rotorcraft models have been exploited in order to represent the trajectory tracking problem as the control of two subsystems in cascade. A hierarchical control design has then been applied to design a practical flight controller which is easy to implement and to tune. The main drawback of the inner-outer loop-based flight controllers is the lack of stability analysis for the connected closed-loop system. In the next subsection, we address this issue by exploiting advanced control theories on systems in cascade.

3.3 Analysis of the closed-loop system stability

By substituting (8) into (7), the closed-loop system dynamics become

$$\begin{cases} \dot{\chi} = A_1\chi - B_1K_\chi\hat{\chi} + \Delta(\hat{\chi}, e) \\ \dot{e} = A_e e \end{cases} \quad (9)$$

The error $\hat{\chi} = (\hat{z} - z_d, \hat{\upsilon} - \upsilon_d)^T$ can be expressed as a function of the original error χ as follows:

$$\hat{\chi} = (\frac{b}{\hat{b}}z - z_d, \frac{b}{\hat{b}}\upsilon - \upsilon_d)^T = \frac{b}{\hat{b}}\chi + \frac{b-\hat{b}}{\hat{b}}(z_d, \upsilon_d)^T \quad (10)$$

So, the outer-loop dynamics become:

$$\begin{aligned} \dot{\chi} &= A_1\chi - B_1K_\chi[\frac{b}{\hat{b}}\chi + \frac{b-\hat{b}}{\hat{b}}(z_d, \upsilon_d)^T] + \Delta(\hat{b}, \chi, e) \\ &= \underbrace{(A_1 - \frac{b}{\hat{b}}B_1K_\chi)\chi}_{f(\hat{b},\chi)} \underbrace{- \frac{b-\hat{b}}{\hat{b}}B_1K_\chi(z_d, \upsilon_d)^T}_{\varepsilon(\hat{b},z_d,\upsilon_d)} + \Delta(\hat{b}, \chi, e) \end{aligned} \quad (11)$$

Now, the closed-loop dynamics can be expressed in the following form:

$$\begin{cases} \dot{\chi} = f(\hat{b}, \chi) + \varepsilon(\hat{b}, z_d, \upsilon_d) + \Delta(\hat{b}, \chi, e) \\ \dot{e} = A_e e \end{cases} \quad (12)$$

The term $\varepsilon(\hat{b}, z_d, \upsilon_d)$ is mainly due to the parameter estimate error $b - \hat{b}$.

Before proving the stability of the closed-loop system (12), we need the following theorem:

Theorem 3. If the following three assumptions hold, then all the solutions $\chi(t)$ and $e(t)$ of (12) are bounded.

A1. The equilibrium point $e = 0$ is Globally Asymptotically Stable (GAS) and Locally Exponentially Stable (LES).

A2. There exist a positive semi-definite radially unbounded function $V(\chi)$ and positive constants c_1 and c_2 such that for $\|\chi\| \geq c_1$

$$\begin{cases} \dfrac{\partial V}{\partial \chi}[f(\hat{b}, \chi) + \varepsilon(\hat{b}, z_d, \upsilon_d)] \leq 0 \\ \|\dfrac{\partial V}{\partial \chi}\|\|\chi\| \leq c_2 V(\chi) \end{cases} \quad (13)$$

A3. There exist a positive constant c_3 and one class-$\mathcal{K}$ function $\gamma(.)$, differentiable at $e = 0$, such that

$$\|\chi\| \geq c_3 \Rightarrow \|\Delta(\hat{b}, \chi, e)\| \leq \gamma(\|e\|)\,\|\chi\| \quad (14)$$

If in addition, $\dot{\chi} = f(\hat{b}, \chi) + \varepsilon(\hat{b}, z_d, \upsilon_d)$ is GAS, then the equilibrium point $(\chi, e) = (0, 0)$ is GAS.

The proof of Theorem 3 can be found in Kendoul (2007).

Thus, in order to prove the stability of the closed-loop system (12), we need to show/prove that the e-subsystem, the χ-subsystem and the coupling term $\Delta(.)$ satisfy the conditions A1, A2 and A3 respectively.

• *A1. e-subsystem stability:* Since the matrix A_e is Hurwitz, then, the e-subsystem (inner-loop) is GES which is stronger than the GAS property.

• *A2. χ-subsystem stability:* We are interested here, in the stability of the subsystem $\dot{\chi} = f(\hat{b}, \chi) + \varepsilon(\hat{b}, z_d, \upsilon_d)$. It is clear from (11) that if $\hat{b} \to b$, the system $\dot{\chi} = f(\hat{b}, \chi) + \varepsilon(\hat{b}, z_d, \upsilon_d)$ will be GAS. Indeed, for $\hat{b} \to b$, we have $\varepsilon(.) \to 0$ and $f(.) \to A_\chi$, which is Hurwitz. Consequently, the inequalities (13) hold.

Now, let us analyze the stability of the χ-subsystem in the presence of parameter estimate errors, i.e., $\hat{b} \to \bar{b} \neq b$. So, in the following, we will show that the term $\varepsilon(\hat{b}, z_d, \upsilon_d)$ is bounded, the matrix $A_1 - \frac{b}{\hat{b}}B_1K_\chi$ is Hurwitz and the tracking error $\chi(t)$ is bounded. Furthermore, we will prove that the assumption A2. of Theorem 3 is satisfied.

Since $\hat{b}(t) \in [b_{min}, b_{max}]$ (see Theorem 1) and the desired trajectories $(z_d(t), \upsilon_d(t))$ are bounded, then it is trivial to deduce from (11) that $\varepsilon(.)$ is bounded. Then, there exists a positive constant d such that $d = \|\varepsilon(.)\|_\infty$.

We recall that the matrix $A_1 - B_1K_\chi$ is Hurwitz and the term $\frac{b}{\hat{b}}$ is positive and bounded. Due to the structure of the matrices A_1 and B_1 (8), then the matrix $\hat{A}_\chi = A_1 - \frac{b}{\hat{b}}B_1K_\chi$ is also Hurwitz. Therefore, we can write $\dot{\chi} - \hat{A}_\chi\chi = \varepsilon(t)$. The solution of the preceding differential equation is:

$$\chi(t) = \chi(0)e^{\hat{A}_\chi t} + \int_0^t e^{\hat{A}_\chi(t-\tau)}\varepsilon(\tau)d\tau \quad (15)$$

From equation (15), we can show that after a finite time T, we obtain

$$\|\chi(t)\| \leq \|\varepsilon(t)\| \leq d, \forall t \geq T \tag{16}$$

This means that given any initial condition $\chi(0)$, the trajectories $\chi(t)$ converge exponentially to a bounded ball with a radius d. Hence, inequalities (13) hold for $\|\chi\| \geq d$.

• *A3. $\Delta(.)$ growth restriction:* Now, let us analyze if the interconnection term $\Delta(.)$ satisfies the growth condition (14). By recalling (7), we have

$$\|\Delta(\hat{\chi}, e)\| = \frac{1}{m}|u(\hat{\chi})|\|H(\hat{\chi}, e)\| \tag{17}$$

where $\|H(\hat{\chi}, e)\| = \sqrt{h_x^2 + h_y^2 + h_z^2}$ and $|u(\hat{\chi})| = m\|\nu(\hat{\chi}) + ge_3\| = m\sqrt{\nu_x^2 + \nu_y^2 + (\nu_z + g)^2}$.

Lemma 4. Assume that the desired trajectories $(z_d(t), \upsilon_d(t))$ and their time-derivatives are bounded. Then, there exist positive constants r, k_1 and k_2 such that the collective thrust $u(\hat{\chi})$ and the coupling term $H(\hat{\chi}, e)$ satisfy the following properties:

$$\begin{aligned} |u(\chi)| &\leq \begin{cases} k_1\|\hat{\chi}\|, & \text{for } \|\hat{\chi}\| \geq r \\ k_1 r, & \text{for } \|\hat{\chi}\| < r \end{cases} \\ \|H(\hat{\chi}, e)\| &\leq k_2\|e\| \end{aligned} \tag{18}$$

Due to space limitation, the proof of Lemma 4 has been omitted here. However, a detailed proof can be found in Kendoul (2007).

Recalling (17) and (18), the interconnection term $\Delta(.)$ verifies

$$\|\Delta(\hat{\chi}, e)\| \leq \frac{k_1 k_2}{m}\|e\|\|\hat{\chi}\|, \quad \text{for } \|\hat{\chi}\| \geq r \tag{19}$$

Substituting (10) into (19) and recalling that $\hat{b}$ and (z_d, υ_d) are bounded, then one can write

$$\begin{aligned} \|\Delta(\hat{b}, \chi, e)\| = \|\Delta(\hat{\chi}, e)\| &\leq \frac{k_1 k_2}{m}\|e\|\|\frac{b}{\hat{b}}\chi + \frac{b - \hat{b}}{\hat{b}}(z_d, \upsilon_d)^T\| \\ &\leq \frac{k_1 k_2}{m}\|e\|(k_3\|\chi\| + k_4\|\chi\|) \leq \frac{(k_1 k_2)(k_3 + k_4)}{m}\|e\|\|\chi\| \end{aligned} \tag{20}$$

for $\|\chi\| \geq 1$, $k_3 = \frac{b}{b_{min}}$ and k_4 is the upper bound of $\|\frac{b-\hat{b}}{\hat{b}}(z_d, \upsilon_d)^T\|$. By defining $\gamma(\|e\|) = \frac{(k_1 k_2)(k_3 + k_4)}{m}\|e\|$, which is a class-$\mathcal{K}$ function, the interconnection term $\Delta(\hat{b}, \chi, e)$ satisfies the growth restriction (14), that is, $\Delta(\hat{b}, \chi, e) \leq \gamma(\|e\|)\|\chi\|$ for $\|\chi\| \geq c_3 \triangleq \max(\frac{r - k_4}{k_3}, 1)$.

Finally, the stability of the closed-loop system (12) and the boundedness of trajectories $(\chi(t), e(t))$ are direct consequences of Theorem 3. Furthermore, if the *PE* property is satisfied, then the estimate $\hat{b}(t)$ converges exponentially to the true value b. Therefore, the χ-subsystem is GAS, thereby ensuring the GAS of the equilibrium point $(\chi, e) = (0, 0)$. This result is very interesting because it states that the aircraft velocities and altitude can be accurately recovered and controlled using only visual cues (optic flow) and IMU data. Furthermore, in the presence of significant external disturbances that may probably induce bounded errors in the parameter estimate $\hat{b}$, the stability of the connected closed-loop system holds and the tracking errors remain within a small bounded region. The tracking errors can be significantly reduced by exciting the system

Table 1. Control system parameters

Para.	*Value*	*Parameter*	*Value*
k_z	0.5	$k_\phi,\ k_{\dot{\phi}}$	4, 4
k_{υ_x}	3	$k_\phi,\ k_{\dot{\phi}}$	4, 4
k_{υ_y}	3	$k_\phi,\ k_{\dot{\phi}}$	4, 4
k_{υ_z}	2		

(*PE* property) in order to improve the estimation of the unknown parameter b. The overall block diagram of the designed adaptive vision-based controller is shown in Fig. 1.

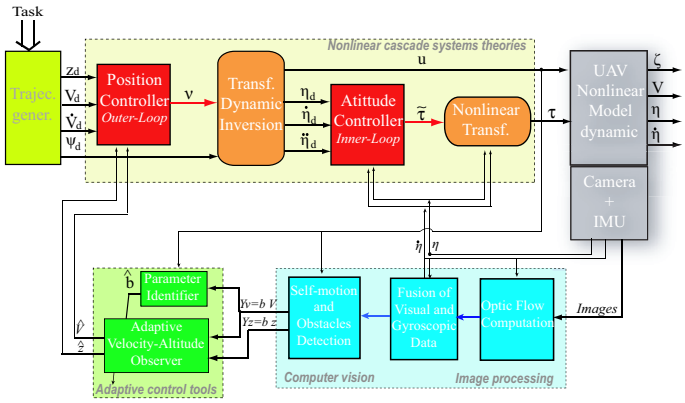

Fig. 1. The overall diagram of the adaptive vision-based autopilot

4. SIMULATION RESULTS

The performances of the adaptive vision-based controller are evaluated using a nonlinear model of the quadrotor UAV. We have performed various simulation tests for achieving useful navigational tasks such as hovering, take-off, vertical landing, aggressive rectangular trajectory tracking, etc (see Kendoul (2007) for more details). Only two experiments are presented here, hovering flight and circular trajectory tracking. The proposed controller was implemented as shown in Fig. 1, and its robustness with respect to noise and external disturbances is analyzed. The values of the controller gains are listed in Table 1.

• *Stabilization and hovering:* the control objective is to stabilize the UAV velocity and attitude and make the rotorcraft hover at the desired altitude $z_d = 10\ m$. The initial conditions are $z(0) = 5m, \upsilon(0) = (4, -1, 2)^T, \eta(0) = (0, 0.3, 0.5)^T$ and $\dot{\eta}(0) = (0, 0, 0)^T$. The true value of the unknown parameter is $b = 3$. As shown on Figs. 2 and 3, the UAV translation and orientation are stabilized and the aircraft performs a hovering flight at the desired altitude of 10 m. Moreover, the parameter estimate $\hat{b}(t)$ converges to its true value after a short transient time.

• *Trajectory tracking:* in this test, the UAV was tasked to climb and fly in a horizontal circle at a desired altitude of 19 m. Moreover, it has to track the reference velocity trajectories $(\upsilon_{x_d}, \upsilon_{y_d}, \upsilon_{z_d})$, starting from the initial configuration $(z(0), \upsilon_x(0), \upsilon_y(0), \upsilon_z(0)) = (10, 0, 0, 0)$ and $(\eta(0), \dot{\eta}(0)) = (0, 0)$. High-fidelity simulation tests have been considered with noisy measurements and external disturbances $F_{ext} = (0.1, 0.1, 0.1\ N)$. In this case, the true value of b was chosen to be 0.5. The obtained results, shown in Figs. 4 and 5 are very satisfactory. Indeed, the reference velocity trajectories are tracked with high

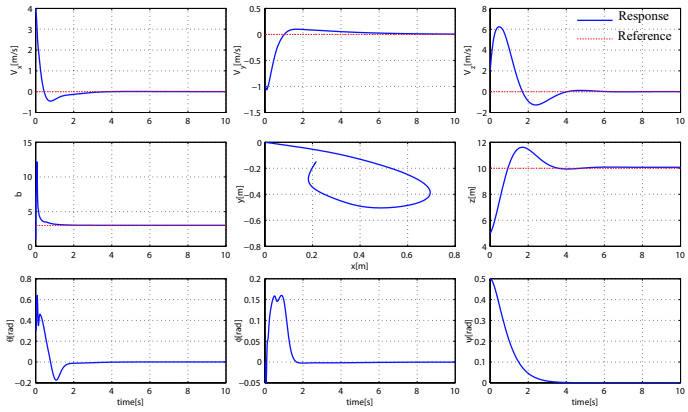

Fig. 2. Stabilization and hovering at a desired altitude

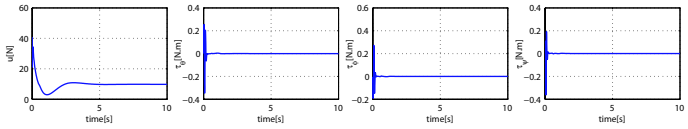

Fig. 3. Control inputs (hovering)

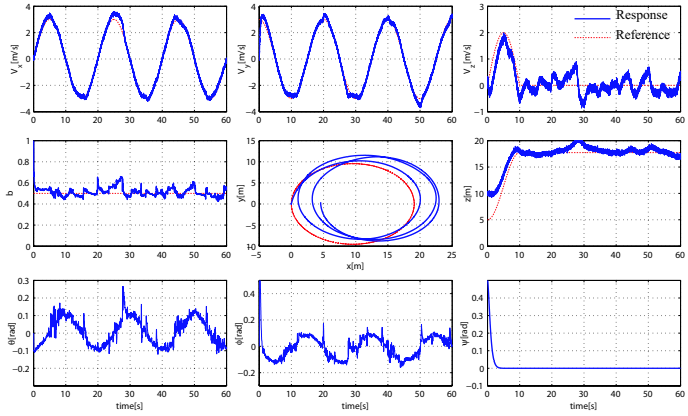

Fig. 4. Circle trajectory tracking in the presence of noise and external disturbances

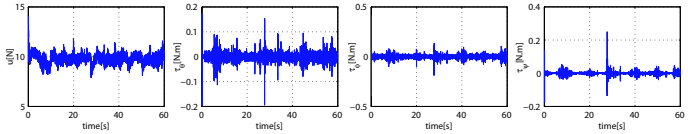

Fig. 5. Control inputs (trajectory tracking)

accuracy. Since the UAV position (x, y) is not controlled, then small drifts in horizontal position occur which are mainly due to the external disturbances.

5. CONCLUSION

In this paper, we have presented the design of a rotorcraft UAV control system that relies on IMU data and useful information extracted from optic flow. Unlike most existing biomimetic flight controllers which are usually used for reactive behaviours, the proposed vision-based autopilot extends optic flow-based control capabilities to complex navigational tasks such as hovering at some desired altitude and arbitrary trajectory tracking. These capabilities are mainly due to the incorporated adaptive mechanism that allows the identification of the unknown scale factor and the recovery of the aircraft absolute velocities and altitude. A practical hierarchical flight controller is then designed. Furthermore, the stability of the connected closed-loop system has been proven by exploiting systems in cascade control theories.

The simulation tests, performed under realistic conditions that include measurements noise and external disturbances, have shown the good performance of the proposed adaptive control system. Indeed, simulation results over various ranges of the flight envelope illustrate that the proposed controller performs very well and the tracking errors remain within a small bounded region. In situations where external disturbances become very significant, tracking errors increase but the stability of the closed-loop system is guaranteed. The major factor that can deteriorate the control performance is the parameter estimate errors, which are mainly due to external disturbances. This issue can be easily overcome by using the accelerometers data in the identification process. Hence, the estimation errors will be reduced, thereby improving significantly the control performance.

REFERENCES

O. Amidi, T. Kanade, and K. Fujita. A visual odometer for autonomous helicopter flight. *Robotics and Autonomous Systems*, 28(2-3):185–193, 1999.

S.M. Ettinger, M. C. Nechyba, P. G. Ifju, and M. Waszak. Vision-guided flight stability and control for micro air vehicles. *Advanced Robotics*, 17(7):617–640, 2003.

W.E. Green, P.Y. Oh, and G. Barrows. Flying insects inspired vision for autonomous aerial robot maneuvers in near-earth environments. In *Proc. of the IEEE Int. Conf. on Robotics and Automation*, pages 2347–2352, New Orleans, April 2004.

P. Ioannou and J. Sun. *Robust Adaptive Control*. Prentice Hall Inc, 1996.

F. Kendoul. Modelling and control of unmanned aerial vehicles, and development of a vision-based autopilot for small rotorcraft navigation. *PhD Thesis Report, Université de Technologie de Compiègne (UTC, CNRS), France*, 2007.

F. Kendoul, I. Fantoni, and G. Dherbomez. Three nested Kalman filters-based algorithm for real-time estimation of optical flow, UAV motion and obstacles detection. In *Proc. of the IEEE Int. Conf. on Robotics and Automation*, pages 4746–4751, Roma, Italy, April 2007.

F. Ruffier and N. Franceschini. Optic flow regulation: the key to aircraft automatic guidance. *Robotics and Autonomous Systems*, 50(4):177–194, 2005.

S. Saripalli, G.S. Sukhatme, L.O. Mejias, and P.C. Cervera. Detection and tracking of external features in an urban environment using an autonomous helicopter. In *Proc. of the IEEE Int. Conf. on Robotics and Automation*, pages 3972–3977, Barcelona, April 2005.

O. Shakernia, R. Vidal, C. Sharp, Y. Ma, and S. Sastry. Multiple view motion estimation and control for landing an unmanned aerial vehicle. In *Proc. of the IEEE Int. Conf. on Robotics and Automation*, pages 2793–2798, Washington DC, 2002.

M. V. Srinivasan, S.W. Zhang, M. Lehrer, and T.S. Collett. Honeybee navigation en route to the gaoal: Visual flight control and odometry. *The Journal of Experimental Biology*, 199(1):237–244, 1996.

J.C. Zufferey and D. Floreano. Fly-inspired visual steering of an ultralight indoor aircraft. *IEEE Transactions On Robotics*, 22(1):137–146, 2006.